INTERNATIONAL JOURNAL OF AUTOMOTIVE AND MECHANICAL ENGINEERING (IJAME)
ISSN: 2229-8649 e-ISSN: 2180-1606
VOL. 19, ISSUE 2, 9634 – 9646
DOI: https://doi.org/10.15282/ijame.19.2.2022.01.0743

ORIGINAL ARTICLE

Optimization of the Performances of a Two-Joint Robotic Arm using Sliding Mode Control

Ahmed Bendimrad*, Ayoub El Amrani and Bouchta El Amrani

Laboratory of Mathematics, Modeling and Applied Physics, Sidi Mohamed Ben Abbellah University, Fez, 30000, Morocco

ABSTRACT – In this paper, we worked on the control of the angular position of a two-joint robotic arm by the sliding mode technique, after having establishing the dynamic equations of the system by the Lagrange method, with the purpose of improving the performances of the system by acting on certain parameters related to the sliding mode technique. The simulation results show an optimization of the sliding mode controller parameters, generally, in the response of the controlled system, which consists on minimizing error and settling time, and eliminating the unwanted phenomenon of chattering, after finding the optimal values of these parameters. Verification by simulation of the robustness of the optimized robotic arm shows that its response is independent of the dimensions and masses of the bodies of this robotic arm, as well as of the applied load. this answer always corresponds to the best performances of speed, settling time and margin of error. the only quantity that varies according to the parameters of the robotic arm and the applied load is the torque required. This couple has a compensating effect to the change of these internal parameters and of this applied load, to keep the same optimal response on the condition of communicating these changes with the controller.

ARTICLE HISTORY
Received: 2nd Aug 2021
Revised: 26th Jan 2021
Accepted: 15th May 2022
Published: 28th June 2022

KEYWORDS
Robotic arm;
Sliding mode;
Control;
Actuator;
Simulation

INTRODUCTION

A robotic arm with two-degree of freedom is a classic example of a simple nonlinear multi-input multi-output (MIMO) dynamic system in robotic literature. It represents a benchmark for testing and evaluating the performance of different control concepts and has been utilized by several researchers to study and compare various control schemes [1]. Compared to other control methods, SMC can offer various good properties, such as simplicity, high robustness to external disturbances and low sensitivity to variations in system parameters [2]. For this reason, we chose the sliding mode control to control our system, which consists of a robotic arm with two joints. Sliding mode control (SMC) is a popular nonlinear control method that drives state trajectories to predefined sliding surfaces, using discontinuous control inputs [2]. However, due to the discontinuous nature of the SMC law, it can produce what is known as the chattering effect, i.e. high-frequency oscillations of the controlled variable, which can disrupt the controlled system or significantly limit the life cycle of the actuators.

Several solutions have been proposed to mitigate this phenomenon [3]. Among the solutions suggested in the literature, it is to approximate the discontinuous control of the SMC by a continuous control. This solution, which has the effect of limiting the tracking error, practically decreases the efficiency of the SMC because of the generation of a pseudo-sliding mode instead of an ideal sliding mode [3]. Another solution to mitigate chattering is to use the higher-order sliding mode control approach, which consists in confining the discontinuity to a derivative of the control variable; thus, this sliding mode involves in addition to the sliding variable, these derivatives with respect to time up to a given order. This approach is suitable for application to electromagnetic or mechanical systems because of its continuous nature of control action [3].

There are several related works in the literature that discuss the sliding mode controller and its applications. For example, previous authors [1] made a comparison between the SMC controller and the PID controller and obtained results that show that the SMC has a faster and robust response compared to the PID controller but with a larger control signal. In [2], three types of non-singular terminal sliding mode controllers were applied on a robotic arm with external disturbances and verified by simulation results, the effectiveness of the proposed modifications for the improvement of convergence rate of the controller, and the reduction of the control input signal. Another work is on an integrated second order SMC controller and the use of an algorithm for the design of the control scheme of manipulator robots, evaluation of the applicability of the proposed controller in a practical way, and confirming the effectiveness in convergence and robustness of the proposed algorithm, by satisfactory results obtained by experiments on a real industrial robot [3].

Our work is based on a simple SMC controller that we have optimized to give its best performances at a constant gain for a two-joint robotic arm. We tested it by simulation for effectiveness in optimizing the response time, the position error and torque provided for a given movement, and in suppressing the chattering phenomenon that the control signal of the SMC usually experiences. In this paper, we start with a theoretical study of the controlled system and the sliding mode controller (SMC), then look for optimal parameters to improve the performances of this controller at a constant gain,

*CORRESPONDING AUTHOR | Ahmed Bendimrad | ahmed.bendimrad@usmba.ac.ma

applied to a bi-articular robotic arm, based on simulation results. The optimized controller (SMC) is then tested to verify its robustness against the variation of the internal parameters of the robotic arm and compared with another controller of the literature applied on an equivalent system.

DESCRIPTION AND DYNAMIC MODEL OF THE SYSTEM

System Description

Our studied system is a two-joint robotic arm, so it has two degrees of freedom represented by two joints in the same plane. To simplify the problem, we assimilate this system into a double pendulum formed by two masses m_1 and m_2 fixed by two rigid rods of negligible masses, of lengths l_1 and l_2 and making respectively the angles θ_1 and θ_2 with the vertical [4] as shown in Figure 1. The two joints that vary the angles θ_1 and θ_2 are respectively actuated by the torques τ_1 and τ_2, and we consider that all frictional torques and forces are neglected.

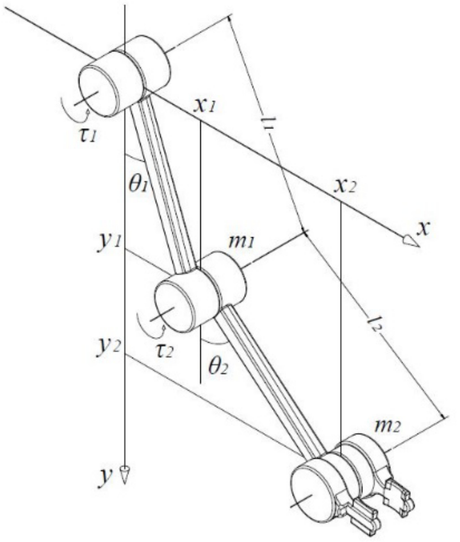

Figure 1. Two-joint robotic arm.

Dynamic model

To model the equations of motion for this system, the Euler-Lagrange equations are applied, taking into account the actuating torques acting on each joint. Since this robotic arm has two degrees of freedom, we have two generalized coordinates θ_1 and θ_2 (as in Figure 1).

$$\begin{cases} x_1 = l_1 \sin\theta_1 \\ y_1 = -l_1 \cos\theta_2 \end{cases}$$
$$\begin{cases} x_2 = l_1 \sin\theta_1 + l_2 \sin\theta_2 \\ y_2 = -l_1 \cos\theta_1 - l_2 \cos\theta_2 \end{cases} \quad (1)$$

The Lagrangian is given by;

$$L = T - V \quad (2)$$

where T is the kinetic energy and V is the potential energy.

$$T = \frac{1}{2} m_1 (\dot{x}_1^2 + \dot{y}_1^2) + \frac{1}{2} m_2 (\dot{x}_2^2 + \dot{y}_2^2)$$
$$V = m_1 g y_1 + m_2 g y_2 \quad (3)$$

After calculations, the Lagrangian is:

$$L = \frac{1}{2}(m_1 + m_2) l_1^2 \dot{\theta}_1^2 + \frac{1}{2} m_2 l_2^2 \dot{\theta}_2^2 + m_2 l_1 l_2 \dot{\theta}_1 \dot{\theta}_2 \cos(\theta_1 - \theta_2) + (m_1 + m_2) g l_1 \cos\theta_1 + m_2 g l_2 \cos\theta_2 \quad (4)$$

We apply the Euler-Lagrange equations [5,6],

$$\frac{d}{dt}\left(\frac{\partial L}{\partial \dot{q}_i}\right) - \frac{\partial L}{\partial q_i} = Q_i \; ; \; i \in \{1,2\} \tag{5}$$

where q_i are the generalized coordinates of the system and Q_i are the generalized forces for the non-conservative forces in the system. In our case, we have $q_i = \theta_i$ and $Q_i = \tau_i$ where τ_i is the actuating torque acting on the joint i. After calculations, we obtain:

$$\begin{aligned} &For\ i = 1: \quad A_1\ddot{\theta}_1 + A_2\ddot{\theta}_2 + A_3\dot{\theta}_2^2 + A_4 = \tau_1 \\ &For\ i = 2: \quad A_1'\ddot{\theta}_2 + A_2\ddot{\theta}_1 - A_3\dot{\theta}_1^2 + A_4' = \tau_2 \end{aligned} \tag{6}$$

where,

$$\begin{aligned} A_1 &= (m_1 + m_2)l_1^2 \\ A_2 &= m_2 l_1 l_2 \cos(\theta_1 - \theta_2) \\ A_3 &= m_2 l_1 l_2 \sin(\theta_1 - \theta_2) \\ A_4 &= (m_1 + m_2) g l_1 \sin\theta_1 \\ A_1' &= m_2 l_2^2 \\ A_4' &= m_2 g l_2 \, sin\, \theta_2 \end{aligned} \tag{7}$$

From Eq. (6), we obtain the following matrix equation:

$$\begin{bmatrix} A_1 & A_2 \\ A_2 & A_1' \end{bmatrix} \begin{bmatrix} \ddot{\theta}_1 \\ \ddot{\theta}_2 \end{bmatrix} + \begin{bmatrix} 0 & A_3\dot{\theta}_2 \\ -A_3\dot{\theta}_1 & 0 \end{bmatrix} \begin{bmatrix} \dot{\theta}_1 \\ \dot{\theta}_2 \end{bmatrix} + \begin{bmatrix} A_4 \\ A_4' \end{bmatrix} = \begin{bmatrix} \tau_1 \\ \tau_2 \end{bmatrix} \tag{8}$$

Equation (8) can be written as follows [7]:

$$M(\theta)\ddot{\theta} + C(\theta, \dot{\theta})\dot{\theta} + g(\theta) = \tau \tag{9}$$

where $M(\theta)$ is the inertia matrix, $C(\theta, \dot{\theta})$ is the Coriolis and centrifugal matrix, $g(\theta)$ is the gravity vector, θ is the angular position vector, $\dot{\theta}$ is the angular velocity vector, $\ddot{\theta}$ is the angular acceleration vector and τ is the input torque vector.

SLIDING MODE CONTROL

A suitable control method is needed to bring the angular position vector of the robotic arm from an initial value to the desired value in a way that is robust with respect to the variation of the system parameters. The control chosen for this is the sliding mode control [8].

Sliding Surfaces

The design of a sliding mode controller starts with the choice of a functions Si defining in the phase space, the sliding surfaces $S_i = 0$ that ensure the convergence of the states i of the system to the desired values. Starting from [8–10], we consider the expression of the functions S_i as follows:

$$S_i = \left(\frac{d}{dt} + \lambda_i\right)^{n-1} e_i \; ; \; i \in \{1,2\} \tag{10}$$

where λ_i is a positive constant, n is the number of times to derive the output to make the command appear (In our case, $n = 2$) and e_i is the error enters the state vector θ_i and the desired state vector θ_{id} where:

$$e_i = \theta_i - \theta_{id} \tag{11}$$

We obtain the following expression of the sliding surfaces:

$$S_i = \dot{e}_i + \lambda_i e_i = 0 \; ; \; i \in \{1,2\} \tag{12}$$

The solution of the equation (12) is the tracking error:

$$e_i(t) = e_i(0)e^{-\lambda t} \tag{13}$$

which tends towards 0 over time. This means that if the trajectory i of the system in the phase space belongs to the surface $S_i = 0$, it will slide on this surface and converge with a speed that depends on λ towards the desired state that corresponds to the origin of the phase space. This sliding regime is obtained by respecting the following invariance condition:

$$\dot{S}_i = 0 \;\; for \;\; S_i = 0 \tag{14}$$

Condition of Sliding Mode Existence

Once the sliding surfaces are established, the existence of the sliding regime must be asserted by ensuring the convergence of the trajectories of the system towards these sliding surfaces for any $t \geq 0$ [11]. For this, we consider the following Lyapunov function [11–16] corresponding to the surface i:

$$V_i = \frac{1}{2}S_i^2 \tag{15}$$

For the trajectories of the system to be stable in the vicinity of the sliding surfaces, the Lyapunove function must be strictly decreasing, hence the following reaching condition:

$$\dot{V}_i = S_i\dot{S}_i < 0 \tag{16}$$

In order for this convergence towards the sliding surfaces from any initial state to be in finite time, the condition (16) is replaced by the following condition, as in [16,17]:

$$S_i\dot{S}_i \leq -K_i|S_i| \tag{17}$$

where K_i are positive constants.

Design of Control Law

We can calculate the control that brings the states of the system to the sliding surfaces and then to the points of equilibrium that correspond to the desired states, by checking the reaching condition in finite time on the one hand, and the invariance condition on the other hand.

$$\begin{cases} S_i\dot{S}_i \leq -K_i|S_i| \; ; \; K_i > 0 \;\; for \; S_i \neq 0 \\ \dot{S}_i = 0 \;\; for \; S_i = 0 \end{cases} \tag{18}$$

To check the conditions (18), we usually choose the expression of $\dot{S}_i$ given by the following reaching law with constant rate [18–20]:

$$\dot{S}_i = -K_i sign(S_i) \;\; ; \;\; K_i > 0 \tag{19}$$

where,

$$sign(S_i) = \begin{cases} -1 \; if \; S_i < 0 \\ 0 \quad if \; S_i = 0 \\ 1 \quad if \; S_i > 0 \end{cases} \tag{20}$$

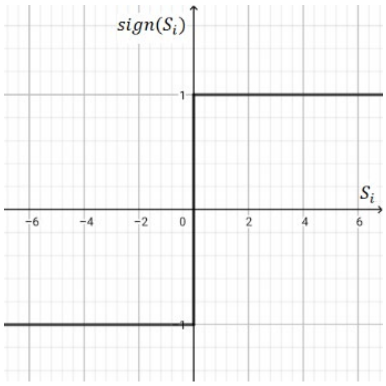

Figure 2. Graphic representation of the sign function $\boldsymbol{sign(S_i)}$.

We replace $\dot{S}_i$ by the derivative of expression (12) of the chosen sliding surface S_i. We obtain,

$$\ddot{\theta}_i - \ddot{\theta}_{i_d} + \lambda_i \dot{e}_i = -K_i.sign(S_i) \tag{21}$$

Moving to the matrix form of Eq. (21), and replacing $\ddot{\theta}$ by its expression from Eq. (9), we obtain:

$$M^{-1}(\theta)\left[\tau - C(\theta,\dot{\theta})\dot{\theta} - g(\theta)\right] - \ddot{\theta}_d + \lambda\dot{e} = -Ksign(S) \tag{22}$$

Where $M^{-1}(\theta)$ always exists, because $det(M(\theta)) \neq 0$ for all l_1, l_2, m_1, m_2, θ_1 and θ_2 ; $\lambda = diag(\lambda_1 , \lambda_2)$ is the slope matrix of the sliding surfaces ; $K = diag(K_1 , K_2)$ is the gain matrix of the discrete control.

Hence, the control vector is given by:

$$\tau = M(\theta)\left[\ddot{\theta}_d - \lambda\dot{e}\right] + C(\theta,\dot{\theta})\dot{\theta} + g(\theta) - M(\theta)Ksing(S) \tag{23}$$

where $M(\theta)$ is positive definite because $A_1 > 0$ and $det(M(\theta)) > 0$.

This control is formed by the sum of a continuous or equivalent control τ_{eq} and a discrete control τ_d [21,22] such that:

$$\begin{aligned} \tau_{eq} &= M(\theta)\left[\ddot{\theta}_d - \lambda\dot{e}\right] + C(\theta,\dot{\theta})\dot{\theta} + g(\theta) \\ \tau_d &= -M(\theta)Ksign(S) \end{aligned} \tag{24}$$

If the system trajectories are outside the sliding surfaces [23], the discrete command τ_d is applied. And if the system trajectories move near the sliding surface [23], the equivalent command τ_{eq} is applied.

Chattering Phenomenon

The studied sliding mode control presents a problem known by the chattering phenomenon, because of the discrete command τ_d. The discontinuity of the function $sign(S)$ of this command leads the state i of the system to the sliding surface S_i by making it switch between the two sides of the neighborhood of this surface. These switches are amplified by the gain K_i of this control, which can lead to strong fluctuations of the control τ [1]. To eliminate or reduce this chattering phenomenon, there is a solution in the literature that consists in smoothing the $sign(S)$ function near the 0 point, replacing it with a continuous function that has a similar appearance, such as the saturation function and the hyperbolic tangent function used in [24]. The general form of the saturation function $sat(S_i/\varphi_i)$ [25,26] and the hyperbolic tangent function $tanh(S_i/\alpha_i)$ [27] is given by:

$$sat\left(\frac{S_i}{\varphi}\right) = \begin{cases} 1 & if \ \ s_i \geq \varphi_i \\ \frac{S_i}{\varphi} & if \ \ |s_i| < \varphi_i \\ -1 & if \ \ s_i \leq -\varphi_i \end{cases} \ ; \ \tanh\left(\frac{S_i}{\alpha_i}\right) = \frac{e^{\frac{S_i}{\alpha_i}} - e^{-\frac{S_i}{\alpha_i}}}{e^{\frac{S_i}{\alpha_i}} + e^{-\frac{S_i}{\alpha_i}}} \tag{25}$$

with $\varphi_i > 0$ and $\alpha_i > 0$.

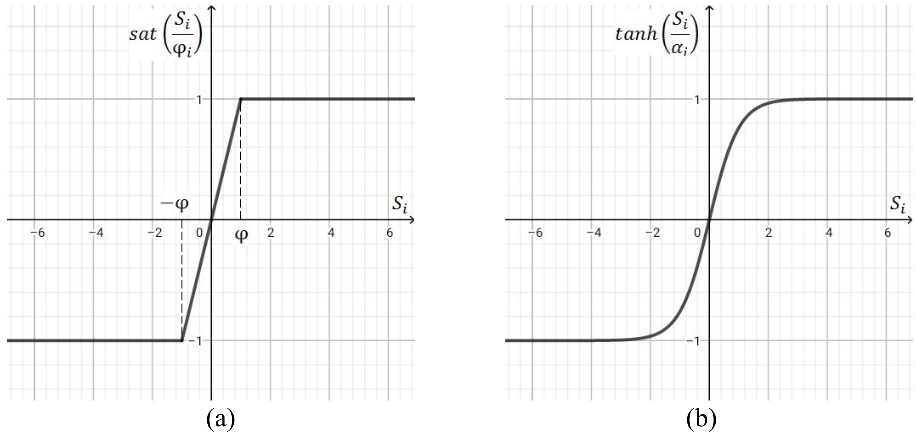

Figure 3. Graphic representation of the (a) saturation function $\boldsymbol{sat(S_i/\varphi_i)}$ and the (b) hyperbolic tangent function $\boldsymbol{tanh(S_i/\alpha_i)}$ for $\boldsymbol{\varphi_i = 1}$ and $\boldsymbol{\alpha_i = 1}$.

SIMULATION RESULTS AND DISCUSSION

We simulated the dynamic model (9) controlled by the sliding mode control (SMC) given by Eq. (23), after replacing the vector $sign(S)$ of the control by a vector $V(S)$ which can take several forms. We obtain the following equation of the command.

$$\tau = M(\theta)[\ddot{\theta}_d - \lambda\dot{e}] + C(\theta,\dot{\theta})\dot{\theta} + g(\theta) - M(\theta)K.V(S) \tag{26}$$

where: $V(S) = [V_1(S_1)\ V_2(S_2)]^T$. We consider in the simulation three forms of the function $V_i(S_i)$: $sign(S_i)$, $sat(S_i/\varphi_i)$ and $tanh(S_i/\alpha_i)$. The block diagram of the controlled dynamic model to be simulated is given by Figure 4.

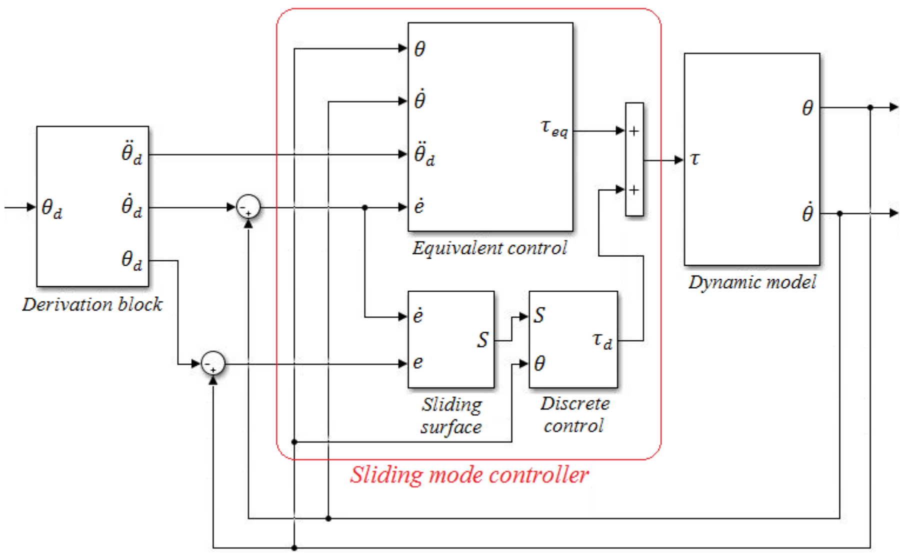

Figure 4. Block diagram of the controlled dynamic model.

This simulation was done in two parts. In the first part, we make a comparison between three controllers, the first one with the function $sign(S_i)$, the second one with the function $sat(S_i/\varphi_i)$, and the third one with the function $tanh(S_i/\alpha_i)$. This comparison is based on the influence of the variation of the different parameters characterizing the control law on the response of the controlled system constituted by the robotic arm in order to determine the most efficient controller.

In the second part, we verify the robustness of the controller obtained related to the variation of the parameters of the robotic arm.

We set the gain matrix K of the sliding mode controllers to: $K = diag(150{,}150)$.

We consider the initial angular position vector: $\theta_{in} = [0\ \ 0]^T\ (deg)$.

We consider the desired angular position vector: $\theta_d = [90\ \ 90]^T\ (deg)$.

Comparison of Three Controllers

The robotic arm parameters taken for this part of simulation are: $l_1 = 1m$; $l_2 = 1m$; $m_1 = 1kg$; $m_2 = 1kg$ and $g = 9.81m.s^{-1}$. For the first controller, $V(S_i) = sign(S_i)$. The response of the system depends only on the slopes λ_i of the sliding surfaces. Figure 5 and Figure 6 show the influence of λ_i on the settling time for 1% band ($t_{s(1\%)}$) of the system and on the maximum absolute value of the control ($max|\tau_i|$) taking $\lambda_i = \lambda_1 = \lambda_2$.

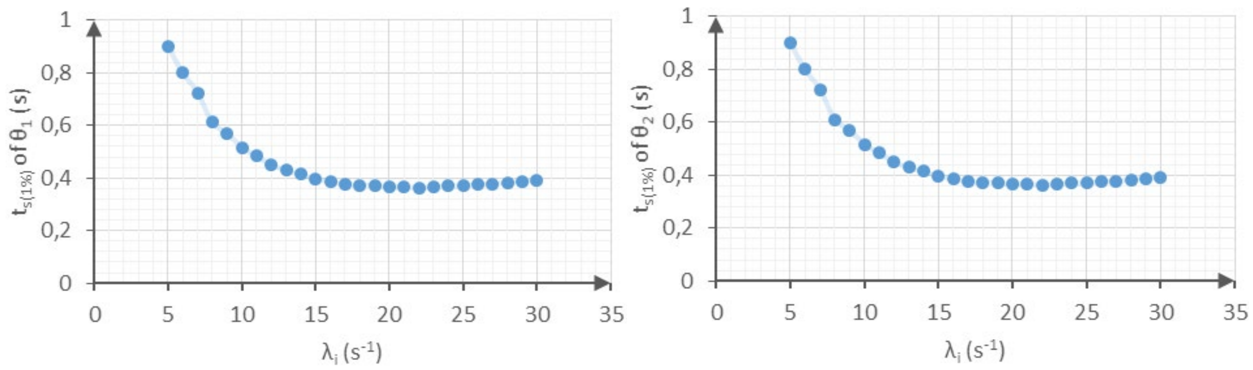

(a) (b)

Figure 5. Vriation of $\boldsymbol{t_{s(1\%)}}$ of (a) $\boldsymbol{\theta_1}$ and (b) $\boldsymbol{\theta_2}$ with $\boldsymbol{\lambda_i}$.

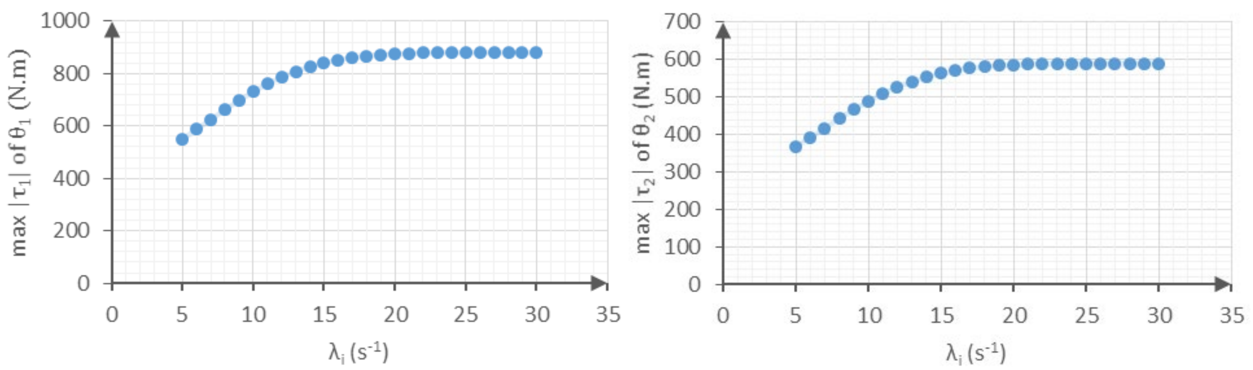

(a) (b)

Figure 6. Vriation of $\boldsymbol{max|\tau_i|}$ of (a) $\boldsymbol{\theta_1}$ and (b) $\boldsymbol{\theta_2}$ with $\boldsymbol{\lambda_i}$.

According to Figure 5, the value of λ_i corresponding to the minimum settling time at 1% for θ_1 and θ_2 is λ_i=22. So, the fastest response for θ_1 and θ_2 is obtained for $\lambda_i = 22$, such that $t_{s(1\%)}(\theta_1) = t_{s(1\%)}(\theta_2) = 0.3635s$. This value for λ_i is in a range where $max|\tau_1|$ and $max|\tau_2|$ have a low rate of change. The simulation shows that θ_1 and θ_2 have the same trajectory at any times (as in Figure 7). The chattering phenomenon of the control is shown in Figure 8.

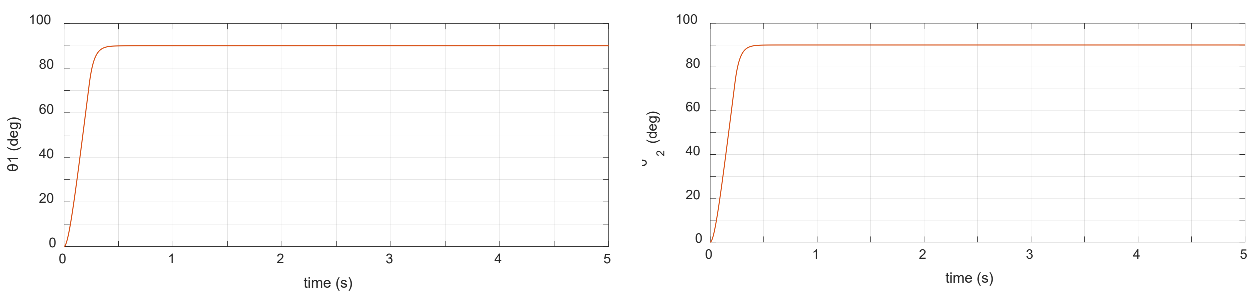

(a) (b)

Figure 7. Trajectory of (a) $\boldsymbol{\theta_1}$ and (b) $\boldsymbol{\theta_2}$ using $\boldsymbol{sign(S_i)}$ for $\boldsymbol{\lambda_i = 22}$.

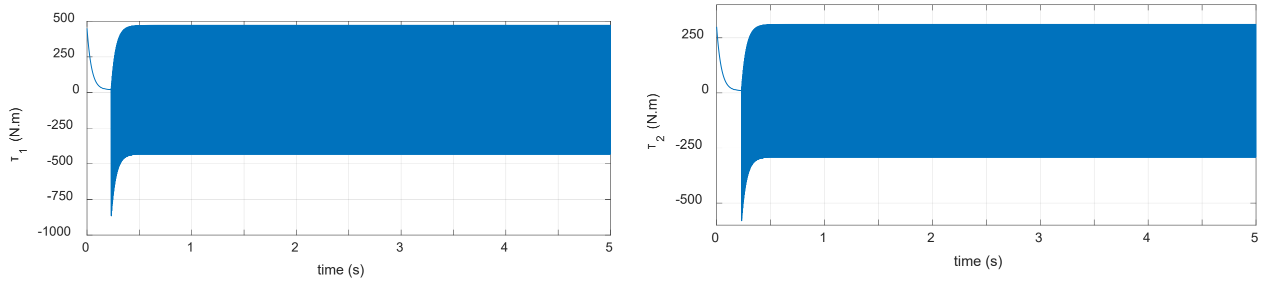

(a) (b)

Figure 8. Torque of (a) $\boldsymbol{\theta_1}$ and (b) $\boldsymbol{\theta_2}$ using $\boldsymbol{sign(S_i)}$ for $\boldsymbol{\lambda_i = 22}$.

For the second controller, $V(S_i) = sat(S_i/\varphi_i)$. We will take $\lambda_i = 22$, so the system response depends only on the parameters φ_i of the control. Figure 9 and Figure 10 show the influence of φ_i on $t_{s(1\%)}$ and on $max|\tau_i|$ taking $\varphi_i = \varphi_1 = \varphi_2$.

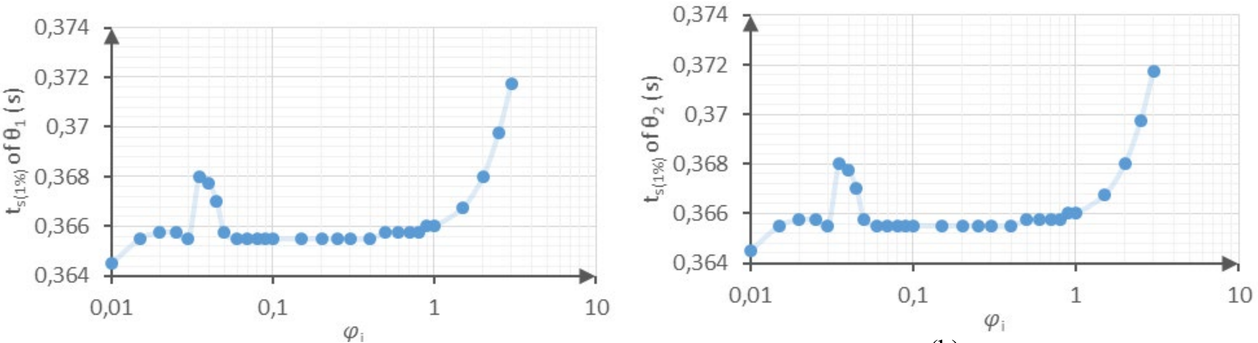

(a) (b)

Figure 9. Variation of $\boldsymbol{t_{s(1\%)}}$ of (a) $\boldsymbol{\theta_1}$ and (b) $\boldsymbol{\theta_2}$ with $\boldsymbol{\varphi_i}$.

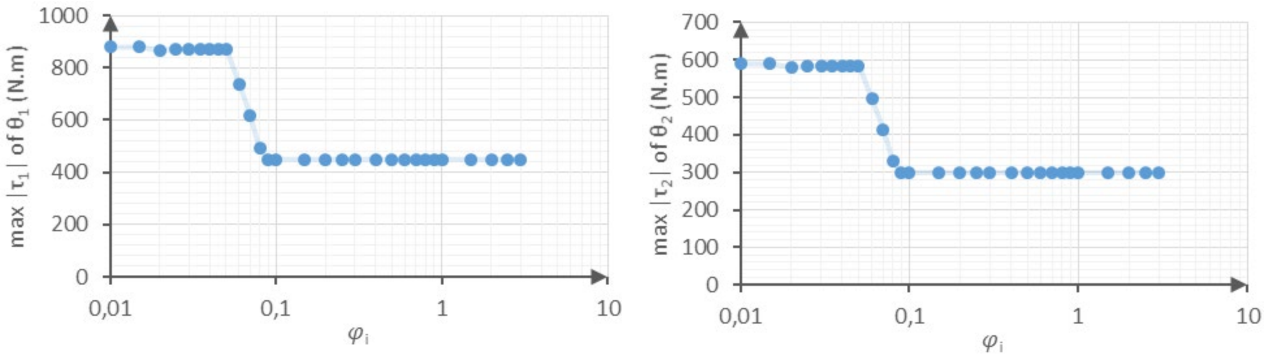

(a) (b)

Figure 10. Variation of $\boldsymbol{max|\tau_i|}$ of (a) $\boldsymbol{\theta_1}$ and (b) $\boldsymbol{\theta_2}$ with $\boldsymbol{\varphi_i}$.

For θ_1 and θ_2, chattering is completely eliminated for $\varphi_i \geq 0.07$, and $t_{s(1\%)}$ and $max|\tau_i|$ remains at minimum values such that $t_{s(1\%)} = 0.3655s$, $max|\tau_1| = 450N.m$, and $max|\tau_2| = 300N.m$ for $0.09 \leq \varphi_i \leq 0.4$. To choose a better value of φ_i, we compare the absolute value of the tracking error $|e|$ at $t = 0.5s$ for $0.09 \leq \varphi_i \leq 0.4$, as presented in Table 1.

Table 1. Absolute value of the tracking error |e| at $\boldsymbol{t = 0.5s}$ for $\boldsymbol{0.09 \leq \varphi_i \leq 0.4}$.

φ_i	0.09	0.15	0.2	0.25	0.3	0.4
$\|e\|$ for $\theta_1\ (deg).10^{-2}$	4.684	4.685	4.686	4.687	4.688	4.692
$\|e\|$ for $\theta_2\ (deg).10^{-2}$	4.684	4.685	4.686	4.687	4.688	4.692

The most accurate answer is obtained for $\varphi_i = 0.09$. The simulation shows that θ_1 and θ_2 have the same trajectory at any time (as in Figure 11). Chattering is completely eliminated from the control as shown in Figure 12.

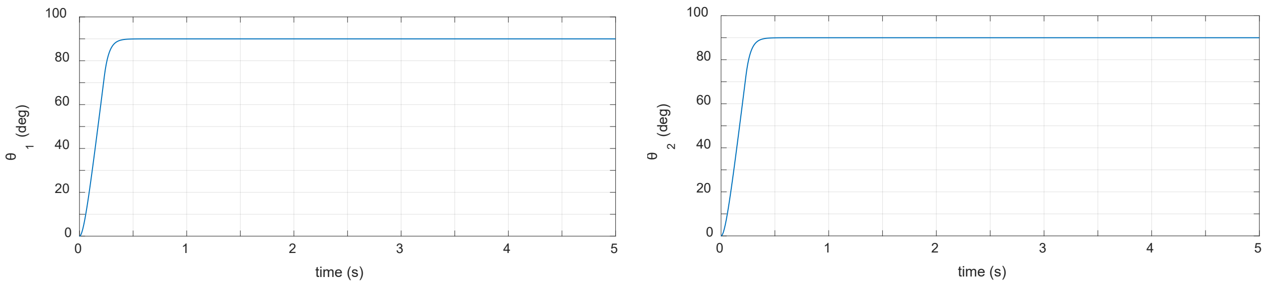

(a) (b)

Figure 11. Trajectory of (a) $\boldsymbol{\theta_1}$ and (b) $\boldsymbol{\theta_2}$ using $\boldsymbol{sat(S_i/\varphi_i)}$ for $\boldsymbol{\lambda_i = 22}$ and $\boldsymbol{\varphi_i = 0.09}$.

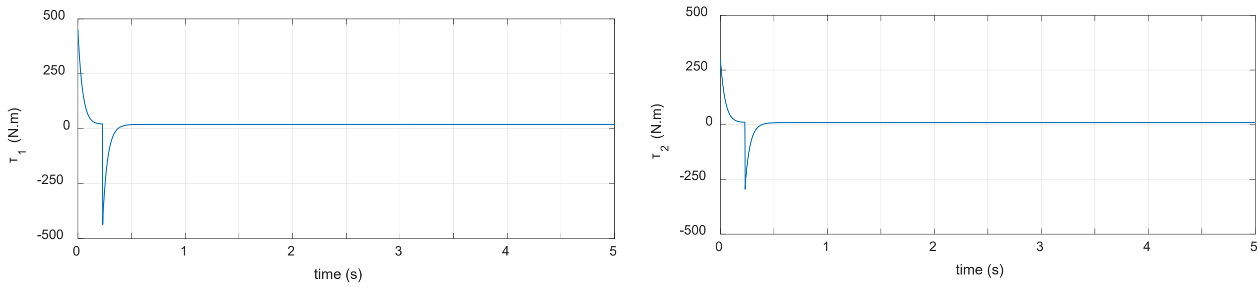

(a) (b)

Figure 12. Torque of (a) $\boldsymbol{\theta_1}$ and (b) $\boldsymbol{\theta_2}$ using $\boldsymbol{sat(S_i/\varphi_i)}$ for $\boldsymbol{\lambda_i = 22}$ and $\boldsymbol{\varphi_i = 0.09}$.

For the third controller, $V(S_i) = tanh(S_i/\alpha_i)$. We also take $\lambda_i = 22$, so the system response depends only on the parameters α_i of the control. Figure 13 and Figure 14 show the influence of α_i on $t_{s(1\%)}$ and on $max|\tau_i|$ taking $\alpha_i = \alpha_1 = \alpha_2$.

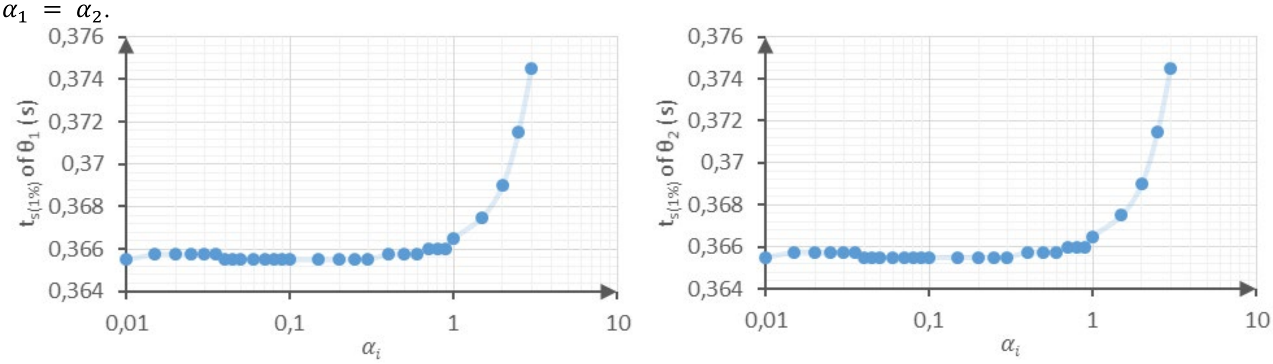

(a) (b)

Figure 13. Variation of $\boldsymbol{t_{s(1\%)}}$ of (a) $\boldsymbol{\theta_1}$ and (b) $\boldsymbol{\theta_2}$ with $\boldsymbol{\alpha_i}$.

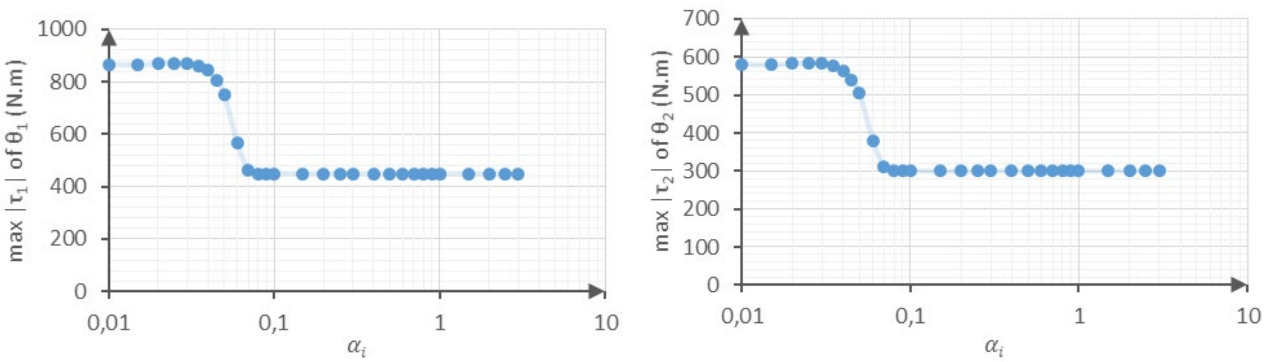

(a) (b)

Figure 14. Variation of $\boldsymbol{max|\tau_i|}$ of (a) $\boldsymbol{\theta_1}$ and (b) $\boldsymbol{\theta_2}$ with $\boldsymbol{\alpha_i}$.

For θ_1 and θ_2, chattering is completely eliminated for $\alpha_i \geq 0.08$, and $t_{s(1\%)}$ and $max|\tau_i|$ remains at minimum values such that $t_{s(1\%)} = 0.3655s$, $max|\tau_1| = 450N.m$, and $max|\tau_2| = 300N.m$ for $0.08 \leq \alpha_i \leq 0.3$. To choose a better value of α_i, we compare the absolute value of the tracking error $|e|$ at $t = 0.5s$ for $0.08 \leq \alpha_i \leq 0.3$, as presented in Table 2. The most accurate answer is obtained for $\alpha_i = 0.08$. The simulation shows that θ_1 and θ_2 have the same trajectory at any time (in Figure 15). Chattering is completely eliminated from the control (Figure 16).

Table 2. Absolute value of the tracking error $|\boldsymbol{e}|$ at $\boldsymbol{t} = \mathbf{0.5}\boldsymbol{s}$ for $\mathbf{0.08} \leq \boldsymbol{\alpha_i} \leq \mathbf{0.3}$.

α_i	0.08	0.11	0.15	0.2	0.25	0.3
$\|e\|$ for $\theta_1\ (deg).10^{-2}$	4.684	4.685	4.686	4.687	4.689	4.691
$\|e\|$ for $\theta_2\ (deg).10^{-2}$	4.684	4.685	4.686	4.687	4.689	4.691

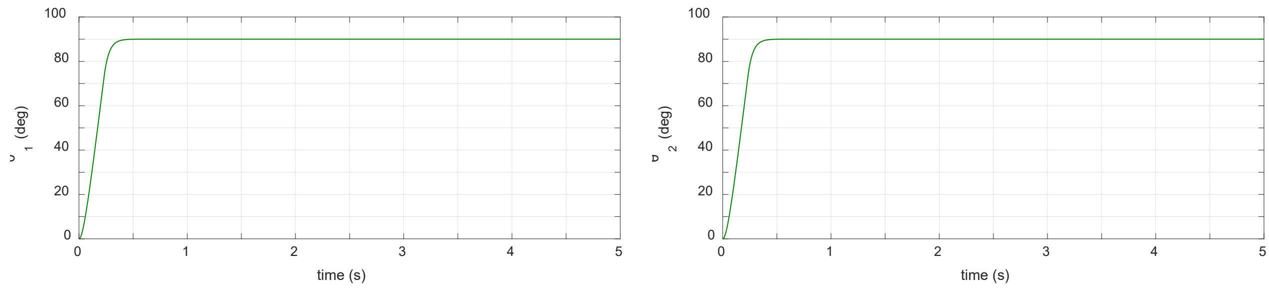

(a) (b)

Figure 15. Trajectory of (a) $\boldsymbol{\theta_1}$ and (b) $\boldsymbol{\theta_2}$ using $\boldsymbol{tanh(S_i/\alpha_1)}$ for $\boldsymbol{\lambda_i} = \mathbf{22}$ and $\boldsymbol{\alpha_i} = \mathbf{0.08}$.

Simulation results show that for $\lambda_i = 22$, $\varphi_i = 0.09$ and $\alpha_i = 0.08$, the sliding mode controller using the $sat(S_i/\varphi_i)$ function and the sliding mode controller using the $tanh(S_i/\alpha_i)$ function have an identical and optimized performances for $max|\tau_i|$, $t_{s(1\%)}$ and $|e|$. We consider the optimized sliding mode controller using the function $sat(S_i/\varphi_i)$ in the following part.

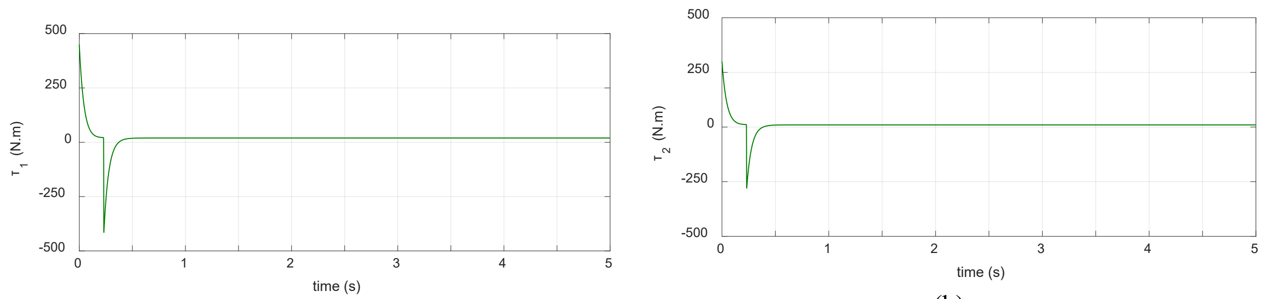

(a) (b)

Figure 16. Torque of (a) $\boldsymbol{\theta_1}$ and (b) $\boldsymbol{\theta_2}$ using $\boldsymbol{tanh(S_i/\alpha_i)}$ for $\boldsymbol{\lambda_i} = \mathbf{22}$ and $\boldsymbol{\alpha_i} = \mathbf{0.08}$.

Verification of the Robustness of The Sliding Mode Controller Obtained

We simulate the response of the robotic arm to the sliding mode controller using the function $sat(S_i/\varphi_i)$, with the parameters: $\lambda_i = 22$ and $\varphi_i = 0.09$, for different values of the parameters of this robotic arm: m_1, m_2, l_1 and l_2, as shown in Table 3. The results are presented in the Figure 17 to Figure 19. According to Figure 17, the angular positions \theta_1 and \theta_2 have the same trajectory at any time and do not depend on the parameters l_1, l_2, m_1 and m_2 of the robotic arm; and therefore, the same applies to the angular velocities \theta_1 and \theta_2 (Figure 18). This verifies the robustness of the used sliding mode controller in relation to the variation of the parameters of the controlled robotic arm.

Table 3. Different combinations of the values chosen for $\boldsymbol{l_1}$, $\boldsymbol{l_2}$, $\boldsymbol{m_1}$ and $\boldsymbol{m_2}$.

	$l_1\ (m)$	$l_2\ (m)$	$m_1\ (kg)$	$m_2\ (kg)$
Case 1	0.1	0.1	0.1	0.1
Case 2	0.1	0.1	0.1	0.5
Case 3	0.1	0.1	0.5	0.1
Case 4	0.1	0.5	0.1	0.1
Case 5	0.5	0.1	0.1	0.1
Case 6	0.1	0.1	0.5	0.5
Case 7	0.5	0.5	0.1	0.1
Case 8	0.1	0.5	0.1	0.5
Case 9	0.5	0.1	0.5	0.1
Case 10	0.5	0.5	0.5	0.5

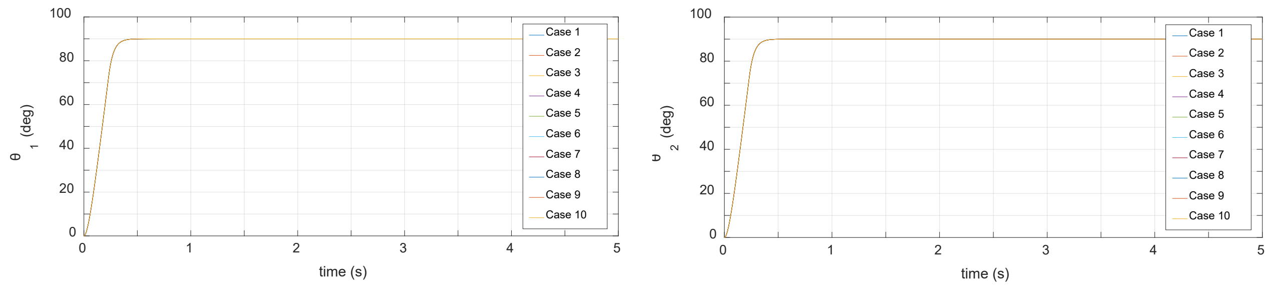

(a) (b)

Figure 17. Trajectories of (a) $\boldsymbol{\theta_1}$ and (b) $\boldsymbol{\theta_2}$ for case 1 to case 10.

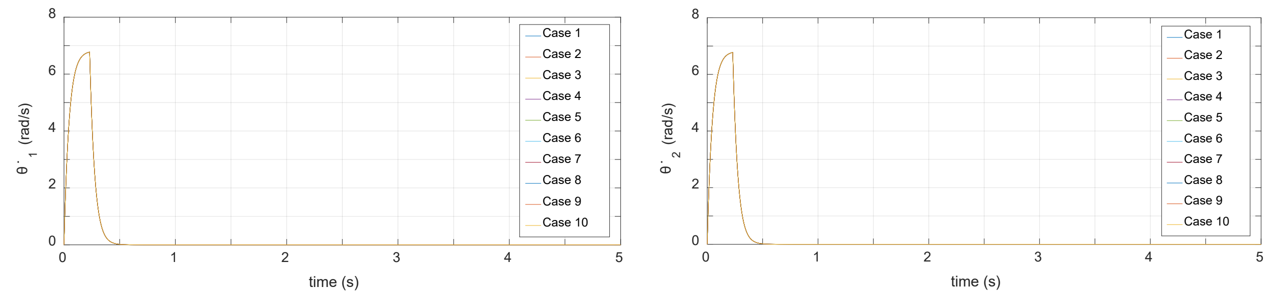

(a) (b)

Figure 18. Trajectories of angular velocity (a) $\boldsymbol{\theta_1}$ and (b) $\boldsymbol{\theta_2}$ for case 1 to case 10.

Figure 19 shows that the torques τ_1 and τ_2 applied, vary according to each combination of the parameters l_1, l_2, m_1 and m_2 of the robotic arm. It means that the used sliding mode controller compensates for variations in the internal robotic arm parameters to always keep the same optimal trajectory of the output to be controlled.

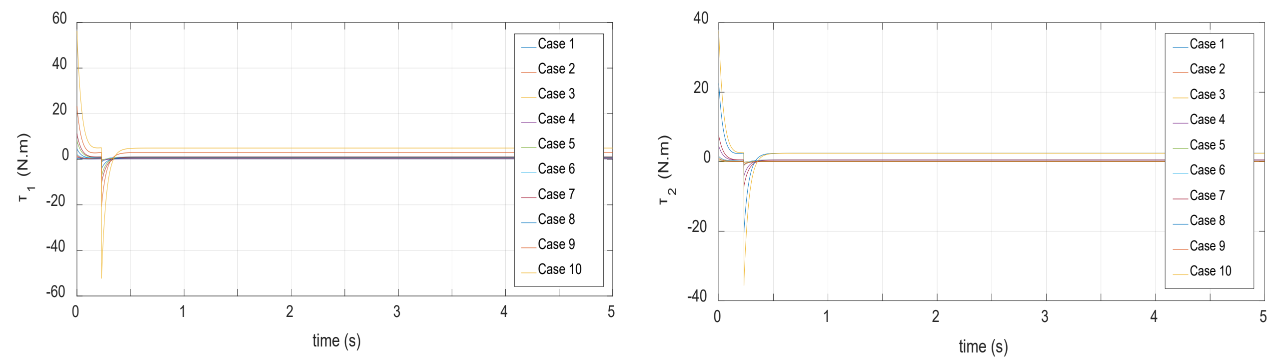

(a) (b)

Figure 19. Torques of (a) $\boldsymbol{\theta_1}$ and (b) $\boldsymbol{\theta_2}$ for case 1 to case 10.

Comparison with Other Results

We compared this optimized SMC controller with the SMC controller of [1] applied on the same robotic arm with the following parameters:

$l_1 = 1m\,;\, l_2 = 1m\,;\, m_1 = 1kg\,;\, m_2 = 1kg$ and $g = 9.81 m.s^{-1}$.

The gain matrix K of the sliding mode controllers: $K = diag(150{,}150)$.

The initial angular position vector: $\theta_{in}[1] = [-90 \quad 90]^T\ (deg)$.

The desired angular position vector: $\theta_d[1] = [90 \quad -90]^T\ (deg)$.

Given the difference between the reference used in our system and that used in the system of [1], we considered the following transformations:

$\theta_1' = \theta_1 - 180\ (deg)$ and $\theta_2' = \theta_2 - \theta_1$

As for our initial system: $\begin{cases} \theta_{in} = [90 \quad 180]^T\ (deg) \\ \theta_d = [270 \quad 180]^T\ (deg) \end{cases}$

and for our transformed system: $\begin{cases} \theta'_{in} = [-90 \quad 90]^T \ (deg) \\ \theta'_d = [90 \quad -90]^T \ (deg) \end{cases}$

Simulation results are shown in Figure 20 and Table 4.

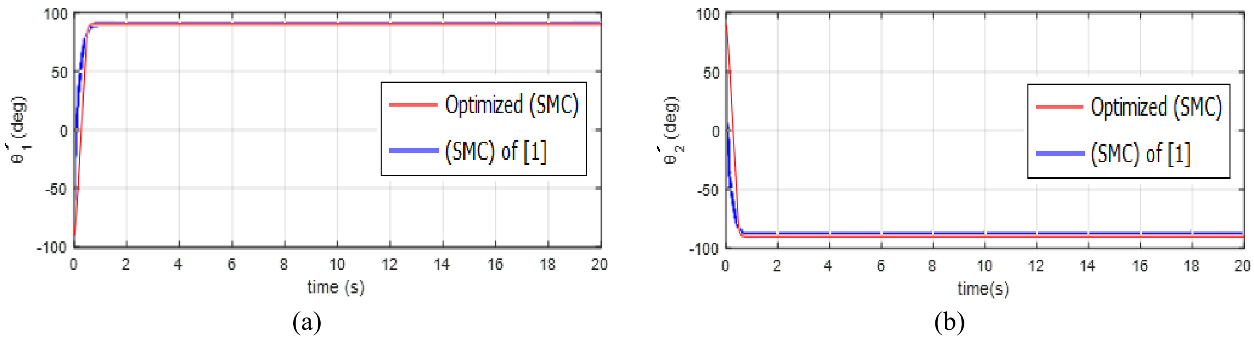

Figure 20. Trajectories of (a) $\boldsymbol{\theta_1}$ and (b) $\boldsymbol{\theta_2}$ for the optimized (SMC), and the (SMC) of reference [1].

Table 4. Comparison of settling time of $\boldsymbol{\theta_1}$ and $\boldsymbol{\theta_2}$ between the optimized (SMC) and the (SMC) of reference [1].

	Optimized (SMC)	(SMC) of [1]
Settling Time for θ_1 (s)	0.546	0.6338
Settling Time for θ_2 (s)	0.546	0.5890

Figure 20 shows a slight improvement in the Settling Time of θ_1 and θ_2 for the optimized (SMC) compared to the (SMC) of [1]. Table 4 ensures this improvement and also shows a synchronization between θ_1 and θ_2 contrary to the (SMC) of [1]. This result is obtained under the assumption that the internal parameters of the robotic arm (l_i,m_i) are perfectly known by the controller at any time, so theoretically, the response is only limited by the maximum torque available. But in practice, this is not the case, hence the need to add a device allowing the instantaneous measurement of these internal parameters to approach this result. In the case of a variable set point, the follow-up of this setpoint is limited by the settling time of the response. Therefore the variations of set point which last less than this settling time are followed only partially.

CONCLUSION

In this paper, a sliding mode control is studied and applied to a two-joint robotic arm, which has been assimilated to a frictionless double pendulum operated by a torque in each joint. The resulting control equation forces the system to follow a sliding surface that causes the system state to tend towards the desired state, hence the robustness of the sliding mode control, but with a chattering phenomenon related to the use of the sign function in control. A solution has therefore been chosen, which consists in replacing the sign function with the saturation function or the hyperbolic tangent function. A simulation was made to compare the effect of each of these two functions on the performance of the sliding mode controller by varying the different parameters related to the control with constant gain. Based on the simulation results, the values of the control parameters that gave the best performance are determined. For these optimal parameters, the saturation function and the hyperbolic tangent function act in the same way on the performance of the control, with complete elimination of the chattering phenomenon. The optimized controller using the saturation function always keeps the same optimized performance for different combinations of lengths and masses of the robotic arm, which verifies the robustness of this controller. The consideration of the incertitude in the parameters of the robotic arm, and external forces applied to this robotic arm in the control, would be an important addition for more efficient operation.

Our future work is the design of a device allowing the measurement of the masses corresponding to the robotic arm in real-time, which allows the application of the sliding mode control in more realistic conditions for this robotic arm, which has, in this case, the ability to compensate for the efforts introduced by the variations of the masses or by the loads applied on the extremity of this robotic arm, in order to have a response near to that of the perfect case where these efforts are supposed to be known.

REFERENCES

[1] A. A. Mohammed and A. Eltayeb, "Dynamics and control of a two-link manipulator using PID and sliding mode control," 2018 Int. Conf. Comput. Control. Electr. Electron. Eng. ICCCEEE 2018, no. August, 2018, pp. 1–5, doi: 10.1109/ICCCEEE.2018.8515795.

[2] J. Geng, Y. Sheng, and X. Liu, "Time-varying non-singular terminal sliding mode control for robot manipulators," *Trans. Inst. Meas. Control*, vol. 36, no. 5, pp. 604–617, 2014, doi: 10.1177/0142331213512367.

[3] A. Ferrara and G. P. Incremona, "Design of an integral suboptimal second-order sliding mode controller for the robust motion control of robot manipulators," *IEEE Trans. Control Syst. Technol.*, vol. 23, no. 6, pp. 2316–2325, 2015, doi: 10.1109/TCST.2015.2420624.

[4] L. J. Chen, “Research on the nonlinear dynamical behavior of double pendulum,” In Proc. 2011 Int. Conf. Mechatron. Sci. Electr. Eng. Comput. MEC 2011, pp. 1637–1640, 2011, doi: 10.1109/MEC.2011.6025792.

[5] J. L. B. Perez and C. F. R. Herrera, “Trajectory tracking control of a double-pendulum System,” 2018 IEEE 2nd Colomb. Conf. Robot. Autom. CCRA 2018, pp. 0–5, 2018, doi: 10.1109/CCRA.2018.8588155.

[6] S. Gao, W. Zhang, W. Kong, H. Ren, and B. Jin, *Force/motion hybrid control of three link constrained manipulator using sliding mode.* vol. 11745 LNAI. Springer International Publishing, 2019.

[7] N. Adhikary and C. Mahanta, “Sliding mode control of position commanded robot manipulators,” *Control Eng. Pract.*, vol. 81, no. December 2017, pp. 183–198, 2018, doi: 10.1016/j.conengprac.2018.09.011.

[8] E. Sarshari, N. Vasegh, M. Khaghani, and S. Dousti, “Sliding mode control in Ziegler’s pendulum with tracking force: Novel modeling considerations,” *ASME Int. Mech. Eng. Congr. Expo. Proc.*, vol. 4 B, pp. 1–6, 2013, doi: 10.1115/IMECE2013-62077.

[9] J. J. E. Slotine and J. A. Coetsee, “Adaptive sliding controller synthesis for nonlinear systems,” *Int. J. Control*, vol. 43, no. 6, pp. 1631–1651, 1986, doi: 10.1080/00207178608933564.

[10] H. Nurhadi, E. Apriliani, T. Herlambang, and D. Adzkiya, “Sliding mode control design for autonomous surface vehicle motion under the influence of environmental factor,” *Int. J. Electr. Comput. Eng.*, vol. 10, no. 5, pp. 4789–4797, 2020, doi: 10.11591/ijece.v10i5.pp4789-4797.

[11] R. Ouiguini, R. Bouzid, and Y. Sellami, “Une commande robuste par mode glissant flou Appliquée à la poursuite de trajectoire d ’ un robot mobile non holonome,” In Conférence Int. sur les Systèmes Télécommunication , d’Electronique Médicale d’Automatique, Cist., 2003, pp. 1–7,.

[12] T. Soehartanto, I. F. Imran, and L. A. Purwitosari, “Control design for direct-drive robotic ARM using sliding mode control,” Proceeding - ICAMIMIA 2017 Int. Conf. Adv. Mechatronics, Intell. Manuf. Ind. Autom., 2018, pp. 277–282,doi: 10.1109/ICAMIMIA.2017.8387601.

[13] M. Guermoui, F. Bouagal and D. Melaab “L ’ utilisation du Modèle de Markov Caché et le Mode Glissant pour la commande vocale des bras manipulateurs,” presented at Int. Conf. Syst. Process. Inf., Guelma, Alger, 2013.

[14] S. Massoum, A. Meroufel, A. Massoum, and W. Patrice, “DTC based on SVM for induction motor sensorless drive with fuzzy sliding mode speed controller,” *Int. J. Electr. Comput. Eng.*, vol. 11, no. 1, pp. 171–181, 2021, doi: 10.11591/ijece.v11i1.pp171-181.

[15] M. Ghafarian, B. Shirinzadeh, A. Al-Jodah, and T. K. Das, “Adaptive fuzzy sliding mode control for high-precision motion tracking of a multi-dof micro/nano manipulator,” *IEEE Robot. Autom. Lett.*, vol. 5, no. 3, pp. 4313–4320, 2020, doi: 10.1109/LRA.2020.2996065.

[16] M. Gharagozloo and A. Shahmansoorian, “Chaos control in gear transmission system using GPC and SMC controllers,” *J. Appl. Comput. Mech.*, vol. 7, no. 1, 2021, doi: 10.22055/JACM.2020.32499.2028.

[17] T. T. Nguyen, “Sliding mode control-based system for the two-link robot arm,” *Int. J. Electr. Comput. Eng.*, vol. 9, no. 4, pp. 2771–2778, 2019, doi: 10.11591/ijece.v9i4.pp2771-2778.

[18] T. L. Nguyen and H. T. Vu, “Super-twisting sliding mode based nonlinear control for planar dual arm robots,” *Bull. Electr. Eng. Informatics*, vol. 9, no. 5, pp. 1844–1853, 2020, doi: 10.11591/eei.v9i5.2143.

[19] S. Ilgen, A. Durdu, E. Gulbahce, and A. Cakan, “Sliding mode control of a two-link robot manipulator using adams matlab software,” In 6th Int. Conf. Control Eng. Inf. Technol. CEIT 2018, no. October, 2018, pp. 25–27, doi: 10.1109/CEIT.2018.8751938.

[20] A. Noordin, M. A. M. Basri, and Z. Mohamed, “Sliding mode control for altitude and attitude stabilization of quadrotor UAV with external disturbance,” *Indones. J. Electr. Eng. Informatics*, vol. 7, no. 2, pp. 203–210, 2019, doi: 10.11591/ijeei.v7i2.1149.

[21] M. Rahmani, H. Komijani, and M. H. Rahman, “New sliding mode control of 2-DOF robot manipulator based on extended grey wolf optimizer,” *Int. J. Control. Autom. Syst.*, vol. 18, no. 6, pp. 1572–1580, 2020, doi: 10.1007/s12555-019-0154-x.

[22] A. Guayasamin, P. Leica, M. Herrera, and O. Camacho, “Trajectory tracking control for aerial manipulator based on lyapunov and sliding mode control,” In Proc. - 3rd Int. Conf. Inf. Syst. Comput. Sci. INCISCOS 2018, vol. 2018-Dec., 2018, pp. 36–41, doi: 10.1109/INCISCOS.2018.00013.

[23] X. Wang and B. Hou, “Sliding mode control of a 2-DOF manipulator with random base vibration based on modified exponential reaching law,” *Vibroengineering Procedia*, vol. 10, pp. 247–252, 2016.

[24] S. Singh and J. Ohri, “Position control of robotic manipulator using SMC under uncertainties,” In 2nd Int. Conf. Recent Adv. Eng. Sci. Manag., no. 3, 2017, pp. 160–169,.

[25] L. Sun and Y. Liu, “Fixed-time adaptive sliding mode trajectory tracking control of uncertain mechanical systems,” *Asian J. Control*, vol. 22, no. 5, pp. 2080–2089, 2020, doi: 10.1002/asjc.2109.

[26] F. Massaoudi, D. Elleuch, and T. Damak, “Robust control for a two DOF robot manipulator,” *J. Electr. Comput. Eng.*, vol. 2019, 2019, doi: 10.1155/2019/3919864.

[27] Y. Ding, C. Liu, S. Lu, and Z. Zhu, “Hyperbolic sliding mode trajectory tracking control of mobile robot,” *Adv. Eng. Res.* vol. 127, pp. 234–238, 2018, doi: 10.2991/eame-18.2018.49.